arXiv:1607.02851v1 [physics.plasm-ph] 11 Jul 2016

Microscopic theory of electron absorption by plasma-facing surfaces

F. X. Bronold and H. Fehske
Institut für Physik, Ernst-Moritz-Arndt-Universität Greifswald, 17489 Greifswald, Germany
(Dated: July 12, 2016)

We describe a method for calculating the probability with which the wall of a plasma absorbs an electron at low energy. The method, based on an invariant embedding principle, expresses the electron absorption probability as the probability for transmission through the wall's long-range surface potential times the probability to stay inside the wall despite of internal backscattering. To illustrate the approach we apply it to a SiO_2 surface. Besides emission of optical phonons inside the wall we take elastic scattering at imperfections of the plasma-wall interface into account and obtain absorption probabilities significantly less than unity in accordance with available electron-beam scattering data but in disagreement with the widely used perfect absorber model.

PACS numbers: 68.49.Jk, 79.20.Hx, 52.40.Hf

I. INTRODUCTION

A surface facing a plasma collects electrons from the plasma more efficiently than it looses electrons due to neutralization of ions and/or de-excitation of radicals. It acquires thus a negative charge triggering in turn an electron-depletion layer in front of it–the plasma sheath–shielding the plasma from the surface. Although known since the beginning of modern plasma physics[1] a quantitative understanding of electron accumulation by plasma walls is still lacking[2]. This is only due partly to unresolved materials science aspects, such as, chemical contamination and/or mechanical destruction of the surface by the plasma. It is also because little is known fundamentally about the interaction of electrons with surfaces at the energies relevant for plasma applications.

Electrons interacting with solid surfaces in the divertor region of fusion plasmas[3], dielectric barrier discharges[4–6], dusty plasmas[7–9], Hall thrusters[10,11], or electric probe measurements[12] have typically energies below 10 eV, much less than the electron energy used in surface analysis[13–15] or materials processing[16]. The energies there are a few 100 eV, an energy range, where the physical processes involved, backscattering and secondary electron emission, are sufficiently well understood[17–24] to make these techniques reliable tools of applied science. Much less is however known about these processes below 100 eV and hence in the energy range relevant for plasmas. In particular, the backscattering probability of a low-energy electron, and closely related to it, the probability with which it is absorbed is basically unknown.

Although electron absorption (sticking) and backscattering are important processes for bounded plasmas there is no systematic effort to determine their probabilities either experimentally or theoretically. The electron sticking probability, for instance, is usually assumed to be close to unity[25–29], irrespective of the energy and angle of incident or the wall material (perfect absorber assumption[30]). The need to overcome this assumption has been strongly emphasized by Mendis[31] but the model calculations he refers to are based on classical considerations not applicable to electrons.

In a recent work[32] we proposed therefore a quantum-mechanical approach for calculating the electron sticking probability. The method is based on two important facts noticed by Cazaux[13]: (i) low-energy electrons do not see the strongly varying short-range potentials of the surface's ion cores but a slowly varying surface potential and (ii) they penetrate deeply into the surface. For Al_2O_3, for instance, the average electron penetration depth at a few eV is around 200Å[33]. The sticking probability for an electron approaching the wall of a plasma can thus be expressed by the transmission probability for the long-ranged surface potential times the probability to remain inside the wall despite of internal backscattering. Essential for our approach is the invariant embedding principle[17,20,24,34]. It allows us to extract from the overwhelming number of electron trajectories the few backwardly directed ones most relevant for sticking. So far we applied the method to MgO[32] obtaining excellent agreement with electron-beam scattering data[35]. In this work we consider SiO_2 finding again good agreement with beam data[36]. In both cases the sticking probability is energy- and angle-dependent as well as significantly less than unity.

The remaining part of the paper is organized as follows. In Section II we describe our microscopic approach for calculating electron absorption and backscattering probabilities in more detail than previously[32], focusing in particular on the invariant embedding principle and its linearization making the approach numerically very efficient. Section III presents results for SiO_2, an in-depth discussion of the model we proposed for the description of imperfect plasma-wall interfaces, and a calculation of orbital-motion limited grain charges beyond the perfect absorber model for electrons. Concluding remarks are given in Section IV.

II. FORMALISM

The method we developed for calculating the probability with which a low-energy electron is absorbed by a surface is general[32]. It can be applied to metallic as well as dielectric surfaces. To be specific we consider in this

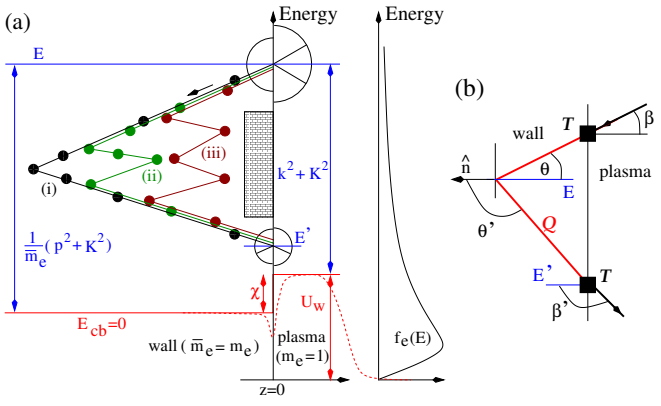

Figure 1. (a) (color online) Interface model used in our calculation. The surface potential (dashed red line) is approximated by a potential step of height χ (solid red line). Three scattering trajectories (i)–(iii) due to emission of optical phonons inside the wall symbolized by bullets are shown each having the same number of total but a different number of backscattering events and bringing an electron entering the wall at energy E back to the plasma at an energy E'. The half circles denote the moduli of the electron momenta inside and outside the wall. Also shown is the energy distribution $f_e(E)$ the approaching electron may have. (b) Illustration of Eqs. (4)–(5). The potential step leads to a quantum-mechanical transmission probability $\mathcal{T}$ whereas the emission of phonons yields a quantity Q to be obtained from the invariant embedding principle shown in Fig. 2. The pre- and post-collision angles inside (θ, θ') and outside (β, β') the wall are measured with respect to the surface normal $\hat{n}$.

work a dielectric SiO_2 surface as an example.

For a dielectric wall with $\chi > 0$ (positive electron affinity) such as SiO_2 the potential energy of an electron across the plasma-wall interface has roughly the form[37] shown, together with other aspects of our approach, in Fig. 1a. An electron approaching the interface from the plasma has to overcome the wall potential U_w. Once it is inside the wall it occupies the conduction band and sees thus a potential barrier χ. Since it is the kinetic energy of the electron in the immediate vicinity of the interface which determines sticking and backscattering probabilities, while the variation of the wall potential U_w is on the scale of the Debye screening length, much larger than the scale on which the surface potential varies, the relevant part of the electron potential energy is essentially a three-dimensional potential step with height χ and electron mass mismatch $\overline{m}_e = m_e^*/m_e < 1$, where m_e^* is the effective electron mass in the conduction band of the wall and m_e is the bare electron mass, as illustrated by the solid red line in Fig. 1a.

The potential step gives rise to quantum-mechanical reflection and transmission. For the situation shown in Fig. 1a, that is, a wall (plasma) occupying the $z < 0$ ($z > 0$) half space and an energy scale for which $E_{\rm cb} = U_w - \chi \equiv 0$, the transmission probability for an electron coming from the plasma, and having thus a kinetic energy $E - \chi > 0$, is given by[38]

$$\mathcal{T}(E,\xi) = \frac{4\overline{m}_e k p}{(\overline{m}_e k + p)^2} \tag{1}$$

with $k = \sqrt{E-\chi}\,\xi$ and $p = \sqrt{\overline{m}_e E}\,\eta$ the $z-$components of the electron momenta outside and inside the wall. In (1) and the formulae below we measure length in Bohr radii, energy in Rydbergs, and mass in electron masses implying inside the wall the electron mass is simply the mass mismatch $\overline{m}_e$. The signs of k and p in (1) are always the same. We can thus define the direction cosines ξ and η referenced, respectively, to the electron momenta outside and inside the wall, by their absolute values: $\xi = |\cos\beta|$ and $\eta = |\cos\theta|$ (see Fig. 1b for the definition of the angles). This choice is also convenient for the theoretical description of internal backscattering which we address later. Since the potential varies only perpendicularly to the surface the lateral momentum $\vec{K}$ is conserved. Together with the conservation of energy, $E = \chi + k^2 + \vec{K}^2 = (p^2 + \vec{K}^2)/\overline{m}_e$, this leads to

$$1 - \eta^2 = \frac{E-\chi}{\overline{m}_e E}\left(1-\xi^2\right) \tag{2}$$

connecting the direction cosines η and ξ. From (2) follows that an electron approaching the wall with kinetic energy $E - \chi = \vec{K}^2 + k^2 > 0$ enters it only when ξ is larger than

$$\xi_c = \begin{cases} 0 & \text{for } \chi < E < E_0 \\ \sqrt{1 - \frac{\overline{m}_e E}{E-\chi}} & \text{for } E > E_0 \end{cases} \tag{3}$$

with $E_0 = \chi/(1-\overline{m}_e)$. For ξ less than ξ_c the electron is in an evanescent wave with $p^2 < 0$ and thus totally reflected[39]. In addition, the requirement (2) may instantaneously reduce the electron's perpendicular kinetic energy to less then the electron affinity χ once it crossed the interface from the plasma side, that is, $p^2/\overline{m}_e < \chi$ even without inelastic scattering. For mass mismatch $\overline{m}_e < 1$, applicable to SiO_2, MgO, Al_2O_3, this happens when $\xi < \sqrt{1-\overline{m}_e}$. Provided the electron cannot gain energy by inelastic scattering, as it is the case for dielectric walls at room temperature, it will have no chance to ever come back to the plasma.

The transmission probability $\mathcal{T}(E,\xi)$ is not identical with the sticking probability. It captures only the ballistic aspect of electron absorption by the wall and is at best an upper bound to it. Once the electron is inside the wall it suffers elastic as well as inelastic scattering. Both may push the electron back to the interface and, after successfully traversing the surface potential in the reverse direction, eventually back to the plasma. Hence, we expect the sticking probability $S(E,\xi) \le \mathcal{T}(E,\xi)$. To take scattering inside the wall into account we defined $S(E,\xi)$ as the probability of an electron hitting the wall from the plasma with energy E and direction cosine ξ not to return to it after entering the wall and suffering backscattering[32],

$$S(E,\xi) = \mathcal{T}(E,\xi)[1 - \mathcal{E}(E,\xi)] \ , \tag{4}$$

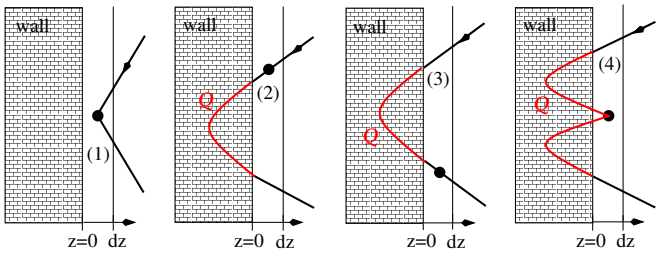

Figure 2. (color online) Schematic illustration of the principle of invariant embedding. Due to the infinitesimally thin additional layer of identical material four additional paths (1)–(4) may contribute to $Q(E\eta|E'\eta')$. However, an infinitesimally thin layer of the same material cannot affect $Q(E\eta|E'\eta')$. Hence, $Q(E\eta|E'\eta')$ has to be invariant against the change the paths (1)–(4) induce leading to Eq. (8).

where

$$\mathcal{E}(E,\xi)=\int_{\eta_{\min}}^{1}d\eta'\int_{E'_{\min}}^{E}dE'\rho(E')\mathcal{B}(E\eta(\xi)|E'\eta')\mathcal{T}(E',\xi(\eta')) \tag{5}$$

is the conditional probability for the electron to escape from the wall after at least one backscattering event. The lower integration limits, $\eta_{\min}=\sqrt{\chi/E}$ and $E'_{\min}=\chi/\eta'^2$, ensure that only events are counted for which the perpendicular post-collision energy $p'^2/\overline{m}_e>\chi$, $\rho(E)=\sqrt{\overline{m}_e^3E}/2(2\pi)^3$ is the conduction band's density of states, and

$$\mathcal{B}(E\eta|E'\eta')=\frac{Q(E\eta|E'\eta')}{\int_0^1 d\eta'\int_0^E dE'\rho(E')Q(E\eta|E'\eta')} \tag{6}$$

is the normalized probability $Q(E\eta|E'\eta')$ for an electron with energy E and direction cosine η to backscatter after an arbitrary number of internal scattering events to a state with energy E' and direction cosine η'. Since the function $Q(E\eta|E'\eta')$ describes backscattering, $0<\theta\leq\pi/2$ and $\pi/2<\theta'\leq\pi$, implying $0\leq\eta,\eta'<1$ as $\eta=|\cos\theta|$. The energy integrals in (5) and (6) anticipate that at room temperature the electron cannot gain energy from a dielectric wall and the functions $\eta(\xi)$ and $\xi(\eta)$ are implicitly defined by (2).

To obtain the quantity $Q(E\eta|E'\eta')$ we employ the invariant embedding principle[17,20,24,34], the essence of it is shown in Fig. 2. For our purpose it is extremely powerful since it focuses from the start on the backscattering trajectories. Compared to forward scattering backscattering is usually much less likely. Constructing thus $Q(E\eta|E'\eta')$, for instance, from the Monte Carlo trajectories mimicking the solution of the electron's Boltzmann equation, obtained under suitable initial and boundary conditions, would be numerically very expensive.

The principle can be derived as follows[24]. Imagine to add to the half space filled with wall material an infinitesimally thin layer of the same material. As a result the four scattering trajectories shown in Fig. 2 may now additionally contribute to $Q(E\eta|E'\eta')$. However, an infinitesimally thin additional layer of the same material cannot change the backscattering properties of the half-space. Hence, $Q(E\eta|E'\eta')$ has to be invariant against this change.

Defining a convolution for functions depending on the variables E,η,E', and η',

$$(A*B)(E\eta|E'\eta')=\int_0^\infty dE''\int_0^1 d\eta''\rho(E'')A(E\eta|E''\eta'')\times B(E''\eta''|E'\eta')\ , \tag{7}$$

summing up the four paths (1)–(4) shown in Fig. 2 (without the transmission/reflection due to the surface potential), and enforcing them not to change $Q(E\eta|E'\eta')$ yields the nonlinear integral equation[24,34]

$$\begin{aligned}&\Big[\frac{\Pi(E)}{\eta}+\frac{\Pi(E')}{\eta'}\Big]Q(E\eta|E'\eta')=G^-(E\eta|E'\eta')\\&+(G^+*Q)(E\eta|E'\eta')+(Q*G^+)(E\eta|E'\eta')\\&+(Q*G^-*Q)(E\eta|E'\eta')\ ,\end{aligned} \tag{8}$$

where the kernels

$$G^\pm(E\eta|E'\eta')=\frac{\delta(E-E'-\omega)}{\eta}K^\pm(E\eta|E'\eta\prime) \tag{9}$$

encode forward (+) or backward (−) scattering. Physically, the lhs describes the reduction of the probability for the electron to follow any one of the old paths, already included in $Q(E,\eta|E',\eta')$, while the rhs corresponds to the four trajectories shown in Fig. 2.

The kernels $G^\pm(E\eta|E'\eta')$ are scattering rates per length. The non-trivial parts $K^\pm(E\eta|E'\eta')$ depend on the scattering process. They can be obtained from the golden rule scattering rate per time dividing it by the pre-collision velocity. Below we consider a SiO_2 surface, where emission of optical phonons dominates the scattering, leading to[32]

$$\begin{aligned}K^\pm(E\eta|E'\eta')=\frac{1}{2\rho(E)}\big[&(E+E'\mp2\sqrt{EE'}\eta\eta')^2\\&-4EE'(1-\eta^2)(1-\eta'^2)\big]^{-1/2}\ .\end{aligned} \tag{10}$$

The function $\Pi(E)$ also entering (8) describes the rate per length to make any collision. For phonon emission it is given by $\Pi(E)=\operatorname{arcosh}(\sqrt{E/\omega})/E$.

In the general case it is hard to work with (8). At low energies however most scattering processes are forwardly peaked. The larger the change of the propagation direction the less likely the process. It is thus possible to use the backscattering kernel $G^-(E\eta|E'\eta')$ as an expansion parameter controlling an iterative solution of (8). Following Glazov and Pázsit[34] we expand therefore in a first step the solution of (8) in the number of the backscattering events. In a second step we take advantage of the fact that for dielectric surfaces at room temperature scattering arises mainly form the emission of optical phonons

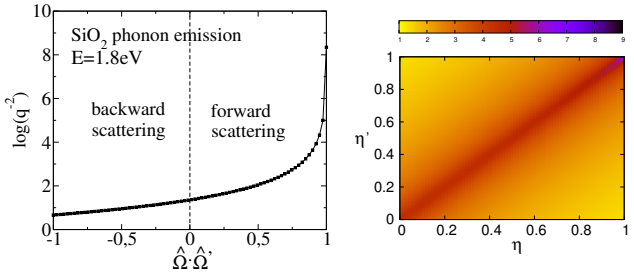

Figure 3. (color online) On the left is shown for SiO_2 and $E = 1.8\,\mathrm{eV}$ the square of the inverse of the momentum transfer q as a function of the cosine of the angle between the pre- and post-collision momenta. It defines at the low electron densities considered in this work the matrix element for phonon emission by the electron entering the wall. The strong forward peaking of the matrix element localizes the forward scattering kernel $K^+(E\eta|E-\omega\eta')$, plotted on the right on a log-scale over the whole range of direction cosines η and η', around the diagonal $\eta = \eta'$. A further consequence of the angle dependence of q is that the backscattering kernel $K^-(E\eta|E-\omega\eta')$ (not shown) is rather isotropic in the (η, η')-plane.

with energy ω. The electron cannot gain energy by scattering. It can loose at most the energy it initially had when entering the wall. Expanding thus $Q(E\eta|E'\eta')$ also in the number of forward scattering events yields a double series which terminates after a finite number of terms. From the differential scattering cross section for the materials we are interested in, SiO_2, MgO, and Al_2O_3 follows moreover that backward scattering due to emission of optical phonons is at least two orders of magnitude less likely than forward scattering[40]. For SiO_2 this can be seen in the left panel of Fig. 3. Hence, writing[32]

$$Q(E\eta|E'\eta') = \sum_{n=1}^{\infty}\sum_{m=0}^{\infty} Q_m^n(E;\eta|\eta')\delta(E-E'-\omega_m^n) \tag{11}$$

with $\omega_m^n = (n+m)\omega$ we can truncate the summation already after a single backward scattering event, that is, after $n = 1$ leading to a linear recursion[32]

$$\begin{aligned} Q_m^1(E;\eta|\eta') &= F_m(E;\eta|\eta')Q_{m-1}^1(E-\omega;\eta|\eta') \\ &\quad + Q_{m-1}^1(E;\eta|\eta')G_m(E-m\omega;\eta|\eta') \end{aligned} \tag{12}$$

for the expansion coefficients with $m = 1, ..., M_{\mathrm{tot}}$, where $M_{\mathrm{tot}} = \lfloor E/\omega \rfloor - 1$ is the number of forward scattering events at most possible,

$$F_m(E;\eta|\eta') = \frac{K^+(E|E-\omega;\eta)\eta'\rho(E-\omega)}{\eta'\Pi(E)+\eta\Pi(E-(m+1)\omega)}\ , \tag{13}$$

$$G_m(E;\eta|\eta') = \frac{\eta\rho(E)K^+(E|E-\omega;\eta')}{\eta'\Pi(E+m\omega)+\eta\Pi(E-\omega)}\ , \tag{14}$$

and an initialization

$$Q_0^1(E;\eta|\eta') = \frac{\eta' K^-(E\eta|E-\omega\eta')}{\eta'\Pi(E)+\eta\Pi(E-\omega)}\ . \tag{15}$$

In deriving the recursion (12) we assumed forward scattering not to change the direction cosine at all. This is justified because, as shown in the right panel of Fig. 3, the kernel $K^+(E\eta|E'\eta')$ is strongly peaked for $\eta = \eta'$. The directional change due to forward scattering is thus negligible and integrals over the direction cosine containing $K^+(E\eta|E'\eta')$ can be handled by a saddle-point approximation. Forward scattering is then encoded in

$$\begin{aligned} K^+(E|E';\eta) &= \int_0^1 d\bar{\eta} K^+(E\eta|E'\bar{\eta}) = \int_0^1 d\bar{\eta} K^+(E\bar{\eta}|E'\eta) \\ &= \frac{1}{4\rho(E)\sqrt{EE'}}\log\frac{r(E|E';\eta)}{q(E|E';\eta)}\ , \end{aligned} \tag{16}$$

where we used the symmetry of $K^+(E\eta|E'\eta')$ with respect to interchanging η and η' and defined the functions

$$\begin{aligned} r(E|E';\eta) &= \sqrt{[E+E']^2 - 4\sqrt{EE'}(E+E')\eta + 4EE'\eta^2} \\ &\quad + \sqrt{EE'} - (E+E')\eta\ , \end{aligned} \tag{17}$$

$$q(E|E';\eta) = \sqrt{[E-E']^2 + 4EE'\eta^2} - (E+E')\eta\ . \tag{18}$$

We thus end up with a model similar in spirit to the Oswald, Kasper and Gaukler model[41] for multiple elastic backscattering of electrons from surfaces.

Inserting finally (11) for the backscattering probability into (5) and performing the energy integrals yields

$$\mathcal{E}(E,\xi) = \frac{\sum_{m=0}^{M_{\mathrm{open}}}\int_{\eta_{\min}}^1 d\eta'\rho(E-\omega_m^1)Q_m^1(E;\eta(\xi)|\eta')\mathcal{T}(E-\omega_m^1,\xi(\eta'))}{\sum_{m=0}^{M_{\mathrm{tot}}}\int_0^1 d\eta'\rho(E-\omega_m^1)Q_m^1(E;\eta(\xi)|\eta')} = \sum_{m=0}^{M_{\mathrm{open}}}\int_{\eta_{\min}}^1 d\eta' P_m^1(E;\eta(\xi)|\eta') \tag{19}$$

with $M_{\mathrm{open}} = \lfloor (E\eta^2-\chi)/(\eta^2\omega)\rfloor - 1$. Substituting this expression for $\mathcal{E}(E,\xi)$ into Eq. (4) gives the electron sticking probability $S(E,\xi)$ for a clean, homogeneous dielectric wall with positive electron affinity.

Besides $S(E,\xi)$ the backscattering probability is also of interest for plasma modeling. Our approach contains

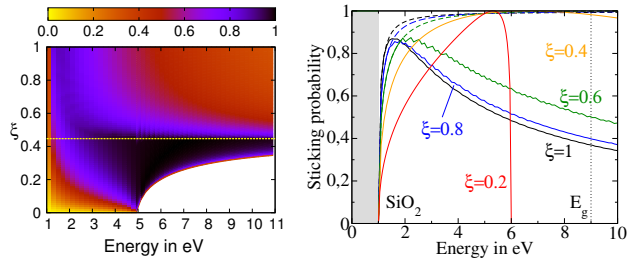

Figure 4. (color online) Angle-resolved sticking probability $S(E,\xi)$ for a clean SiO_2 surface. The left panel shows $S(E,\xi)$ for the whole range of direction cosines ξ and energies $E \leq 11\,\mathrm{eV}$. Total reflection takes place in the white region. Below the yellow dotted line, indicating $\xi = \sqrt{1-\overline{m}_e}$, inelastic backscattering has no effect on the sticking probability. In the right panel $S(E,\xi)$ (solid line) and $\mathcal{T}(E,\xi)$ (dashed line) are plotted as a function of E for representative ξ. The grey area denotes the energy range of the conduction band.

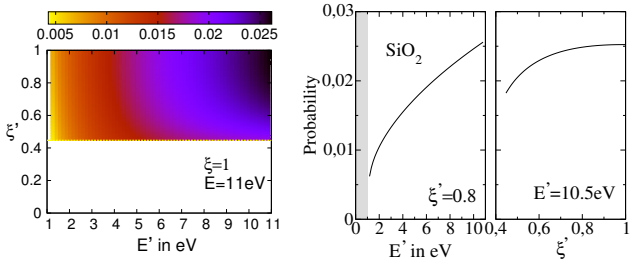

Figure 5. (color online) On the left is plotted the probability $R^1_m(E;\eta(\xi)|\eta')$ for an electron hitting a clean SiO_2 surface with $E = 11\,\mathrm{eV}$ and $\xi = 1$ to backscatter diffusely into a state with direction cosine $\xi' = \xi(\eta')$ and energy E'. Below the dotted yellow line $R^1_m(E;\eta(\xi)|\eta') = 0$ since diffuse backscattering cannot lead to post-collision direction cosines $\xi' < \sqrt{1-\overline{m}_e}$. On the right are shown a horizontal and a vertical cut through the data depicted on the left. Diffuse backscattering peaks around the entrance energy $E = 11\,\mathrm{eV}$ and the entrance direction cosine $\xi = 1$.

two types of backscattering processes: specular quantum-mechanical reflection given by $\mathcal{R}(E,\xi) = 1-\mathcal{T}(E,\xi)$ and diffuse backscattering encoded in

$$R^1_m(E;\eta(\xi)|\eta') = \mathcal{T}(E,\xi)P^1_m(E;\eta(\xi)|\eta') \qquad (20)$$

with $P^1_m(E;\eta(\xi)|\eta')$ defined in (19). The latter gives the probability for an electron hitting the wall with energy E and direction cosine ξ to end up in a state with energy $E' = E - m\omega$ and direction cosine $\xi' = \xi(\eta')$ where η' and ξ' are the post-collision direction cosines inside and outside the wall.

III. RESULTS

We now apply our approach to a SiO_2 surface characterized by $\overline{m}_e = 0.8$[18], $\chi = 1\,\mathrm{eV}$[42], $\omega = 0.15\,\mathrm{eV}$[18], and $E_g = 9\,\mathrm{eV}$[43]. For an actual SiO_2 surface the parameters may deviate from these values depending on material science aspects which we do not address in this work.

Numerical results for $S(E,\xi)$ are shown in Fig. 4. First, we focus on the left panel showing data over the whole range of direction cosines ξ and energies E up to $11\,\mathrm{eV}$. For $E > E_g = 9\,\mathrm{eV}$ our results are only rough estimates since an electron entering the wall at these energies can already create electron-hole pairs across the band gap. This Coulomb-driven process is not included. It can be treated in the same spirit leads however to a recursion containing energy integrals making the numerical treatment more demanding. The white area in the plot for $S(E,\xi)$ indicates the region in the (E,ξ)-plane where total reflection occurs. It is smaller than for MgO[32] because $\overline{m}_e$ is larger for SiO_2. Below the dotted yellow line inelastic backscattering due to emission of phonons is irrelevant for sticking because conservation of lateral momentum and total energy force the perpendicular energy of the electron to drop below the potential step χ once it crossed the interface from the plasma side. It is hence already confined by quantum-mechanical transmission alone. Only above the dotted yellow line inelastic backscattering may bring the electron back to the interface and, after traversing the surface potential in the reversed direction, back to the plasma. Hence, for SiO_2, as well as any other dielectric with mass mismatch $\overline{m}_e < 1$, $S(E,\xi) = \mathcal{T}(E,\xi)$ for $\xi < \sqrt{1-\overline{m}_e}$ and $S(E,\xi) < \mathcal{T}(E,\xi)$ for $\xi > \sqrt{1-\overline{m}_e}$. The sticking coefficient is thus only for some E and ξ equal to the transmission probability. This can be more clearly seen in the right panel of Fig. 4, where $S(E,\xi)$ (solid lines) and $\mathcal{T}(E,\xi)$ (dashed lines) are plotted as a function of E for some representative ξ. To indicate the efficiency of our approach we mention that we obtained the about 3000 data points for $S(E,\xi)$ in Fig. 4, corresponding each to a sum of trajectories with one backward and (depending on energy) up to 80 forward scattering events, with the former interlaced between the latter in all possible ways, in only one hour computing time on a notebook.

The angle- and energy-resolved probability for diffuse backscattering $R^1_m(E;(\xi)|\eta')$ introduced in (20) is depicted in Fig. 5 for $E = 11\,\mathrm{eV}$ and $\xi = 1$. It is largest for $E' = E$ and $\xi' = \xi$. Post-collision direction cosines $\xi' < \sqrt{1-\overline{m}_e}$ are excluded because mass mismatch and conservation of lateral momentum and total energy make them to correspond to internal states with perpendicular energy less than χ. Scattering channels in these directions are thus closed. The maximum of the diffuse backscattering probability is always at the initial energy E and direction cosine ξ. Had we chosen other values for E and ξ the plot would look similar only with a shifted maximum.

Total reflection forces the sticking probability for an electron to vanish if it hits the surface with energy E and direction cosine $\xi < \xi_c$. It is caused by the mass mismatch and the conservation of lateral momentum and total energy. The former holds only for a homogeneous interface. In reality imperfections destroy the homogene-

ity. Lateral momentum will thus not be conserved and total reflection suppressed. To account for this possibility we now include elastic interface scattering along the lines Smith and coworkers used in their theoretical treatment of ballistic electron-emission spectroscopy[44].

Central to the approach is the probability for an electron hitting the wall from the plasma with a kinetic energy $E-\chi > 0$ to make a transition from (E,ξ) to (E',ξ') due to elastic scattering by any of the interfacial scattering centers,

$$P(E|E';\xi) = \frac{C/\xi}{1+C/\xi}\frac{\delta(E-E')}{\sqrt{E-\chi}}\theta(E-\chi)\ , \qquad (21)$$

where C is a parameter proportional to the density of the scatterers and the square of the modulus of the scattering potential which we assume to be independent of the initial and final scattering states (hard core scattering potential). Lacking a detailed knowledge of the structural properties of the interface we use C as a fit parameter. The function $P(E|E';\xi)$ can be derived from the probability to make a transition due to scattering by a single center–given by the ratio of the golden rule scattering rate per time and the rate with which electrons hit the interface–taking interference corrections due to other centers into account[44].

Any physical quantity $f(E,\xi)$ affected by interfacial disorder turns then into

$$\bar{f}(E,\xi) = f(E,\xi)\left[1-\int_0^1 d\xi'\int_\chi^\infty dE'\sqrt{E'-\chi}P(E|E';\xi)\right] + \int_0^1 d\xi'\int_\chi^\infty dE'\sqrt{E'-\chi}P(E|E';\xi)f(E',\xi')\ , \qquad (22)$$

where the first and second term on the rhs stand, respectively, for trajectories without and with interfacial scattering. Using this rule together with

$$\int_0^1 d\xi'\int_\chi^\infty dE'\sqrt{E'-\chi}P(E|E';\xi) = \frac{C/\xi}{1+C/\xi} \qquad (23)$$

yields for the sticking probability of a disordered dielectric wall[32]

$$\bar{S}(E,\xi) = \frac{\mathcal{T}(E,\xi)}{1+C/\xi}[1-\overline{\mathcal{E}}(E,\xi)] + \frac{C/\xi}{1+C/\xi}\int_{\xi_c}^1 d\xi' T(E,\xi')[1-\bar{\mathcal{E}}(E,\xi')]\ , \qquad (24)$$

where $\bar{\mathcal{E}}(E,\xi)$ is given by (5) with $\mathcal{T}(E,\xi)$ replaced by

$$\overline{\mathcal{T}}(E,\xi) = \frac{\mathcal{T}(E,\xi)}{1+C/\xi} + \frac{C/\xi}{1+C/\xi}\int_{\xi_c}^1 d\xi'\mathcal{T}(E,\xi') \qquad (25)$$

and ξ_c defined by (3). Notice, in the limit $C\to 0$ we recover from (24) the sticking probability $S(E,\xi)$ for a clean wall given by (4) while for $C\to\infty$ we obtain the sticking probability for the totally disordered, dirty wall.

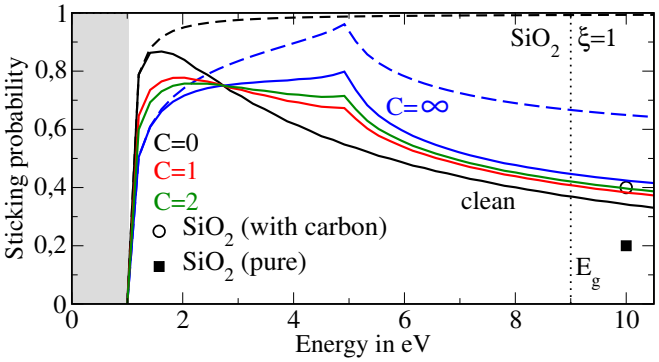

Figure 6. (color online) Sticking probability $\overline{S}(E;1)$ for an electron hitting a SiO_2 surface perpendicularly as obtained from Eq. (24) (solid lines). We show data for $C=0$ (black), 1 (red), 2 (green), and ∞ (blue) with $\overline{\mathcal{T}}(E;1)$ also included for $C=0$ and $C=\infty$ (dashed lines). Symbols are data from electron-beam scattering experiments[36].

The sticking probability $\bar{S}$ of a disordered SiO_2 surface is shown in Fig. 6 for $\xi=1$ (normal incident) and $C=0,1,2$, and ∞. To indicate that our approach captures essential aspects of electron absorption by a surface we also plot data for two types of SiO_2 surfaces obtained from electron-beam scattering experiments[36]. Although the experimental data are in an energy range where electron-hole pair generation already starts to play a role they are nevertheless sufficiently close to the theoretical results to support our modeling approach. They also show that the perfect absorber value, $S(E,\xi)\approx 1$, is not applicable to SiO_2. For MgO experimental data are available for lower energies showing a much better agreement with the theoretical data[32].

Dashed lines show, for comparison, $\overline{\mathcal{T}}(E,1)$, which is the sticking probability in the absence of backscattering. For $C=0$, $\bar{S}(E,1)$ deviates strongly from $\overline{\mathcal{T}}(E,1)$ (black lines), whereas for $C=\infty$ the two quantities approach each other (blue lines). The reason is the angle-averaging at the dirty surface (see Eq. (24)) which lessens, for a fixed ξ, the impact of inelastic backscattering compared to the knock-out of propagation directions by total reflection. The kink in $\bar{S}(E,1)$ at $E=E_0$ signals the knock-out. Comparing the results for MgO ($\overline{m}_e=0.4$)[32] with the results for SiO_2 ($\overline{m}_e=0.8$) indicates moreover that the closer $\overline{m}_e$ to unity the more affected is $\bar{S}(E,1)$ by inelastic backscattering. The mass mismatch $\overline{m}_e$ turns thus out to control $\bar{S}(E,1)$. This is not surprising. Because it is the effective electron mass which subsumes at low energy the elastic scattering of the electron by the ion cores of the wall.

At low energies, the electron-wall interaction in a plasma is usually treated within the perfect absorber model[30] stating that the probability with which an electron is absorbed (backscattered) by the wall is close to unity (vanishes). We have seen however that both probabilities are in fact energy- and angle-dependent and deviate from the perfect absorber values. It is thus of interest

material	m_e^*/m_e	χ[eV]	ω[eV]	interface	$\tilde{s}$	$Q_p[-e]$
SiO_2	0.8	1.0	0.15	clean	0.65	3028
SiO_2	0.8	1.0	0.15	dirty	0.67	3063
Al_2O_3	0.4	2.5	0.10	clean	0.42	2645
Al_2O_3	0.4	2.5	0.10	dirty	0.43	2645
MgO	0.4	1.0	0.10	clean	0.28	2262
MgO	0.4	1.0	0.10	dirty	0.31	2367
PAM	–	–	–	–	1	3446

Table I. Material parameters for the dielectrics used in this work and the orbital-motion limited charge Q_p acquired in an argon plasma with $k_BT_e = 2\,\text{eV}$ and $k_BT_i = 0.026\,\text{eV}$ by dust particles made out of these dielectrics and having radius $R = 1\,\mu\text{m}$. The parameter $\tilde{s}$ defined in Eq. (27) contains the material dependence of the particle charge. As for SiO_2[18,42,43] the material parameters for MgO[45,46] and Al_2O_3[47,48] can be different for actual particles/surfaces due to material science aspects not addressed in this work.

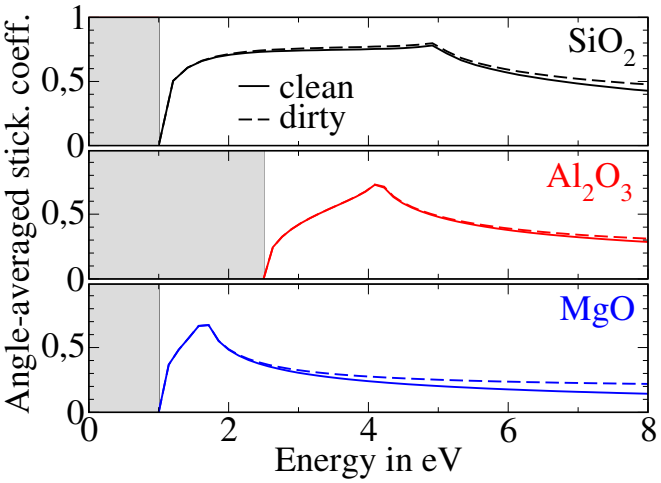

Figure 7. Angle-averaged sticking coefficient $\langle\bar{S}(E,\xi)\rangle_\xi$ for a SiO_2, an Al_2O_3, and a MgO surface. Solid and dashed lines indicate, respectively, $\langle\bar{S}(E,\xi)\rangle_\xi$ for a clean ($C = 0$) and a dirty interface ($C = \infty$). The kink in the data signals the knock-out of propagation directions by total reflection.

to work out the consequences of our results for the modeling of bounded plasmas. As a first plasma application we consider the orbital-motion limited (OML) charging[49] of a dielectric particle in a plasma. Similar results would be however obtained for other charging models as well[50,51].

The grain surface is characterized by $\bar{S}(E,\xi)$ leading to an electron capture cross section $\sigma_c^e(E,\xi) = \bar{S}(E,\xi)\pi R^2(1+eV/E)$ with E and ξ the energy and direction cosine of the incident electron and $V < 0$ the grain's floating potential. The capture cross section yields the flux balance,

$$\tilde{s}\, j_e^{\text{OML}}(V) = j_i^{\text{OML}}(V)\ , \tag{26}$$

where $j_e^{\text{OML}}(V)$ and $j_i^{\text{OML}}(V)$ are the OML fluxes[49] and

$$\tilde{s} = \int_\chi^\infty \frac{dE}{kT_e}\exp\left[-\frac{E-\chi}{kT_e}\right]\frac{E-\chi}{kT_e}\langle\bar{S}(E,\xi)\rangle_\xi \tag{27}$$

with

$$\langle\bar{S}(E,\xi)\rangle_\xi = \int_0^1 d\xi\,\bar{S}(E,\xi) \tag{28}$$

the angle-averaged sticking probability. The (hard) perfect absorber assumption $\bar{S}(E,\xi) = 1$ gives $\tilde{s} = 1$.

In the limit $R \ll \lambda_D$ the grain charge in units of $-e$ is given by $Q_p = -4\pi R\varepsilon_0 kT_eV/ekT_e$ with V the root of (26). Table I shows results for SiO_2, Al_2O_3, and MgO. Besides the expected deviation of the grain charge from the perfect absorber (PAM) charge we also find a material dependence which could be tested by high precision charge measurements[52]. Figure 7 finally shows for SiO_2, Al_2O_3, and MgO the angle-averaged sticking probability $\langle\bar{S}(E,\xi)\rangle_\xi$ entering (27). Since we calculate $\langle\bar{S}(E,\xi)\rangle_\xi$ only up to $E \simeq E_g$, for $E > E_g$ we should have included electron-hole pair generation leading to a more complicated recursion scheme containing energy integrals, we approximate in (27) $\langle\bar{S}(E,\xi)\rangle_\xi$ for $E > E_g$ by its upper bound $\langle\overline{\mathcal{T}}(E,\xi)\rangle_\xi$. The values for $\tilde{s}$ given in Table I are thus only upper bounds.

IV. CONCLUSION

We described a method to calculate from a microscopic model the sticking and backscattering probabilities for a low-energy electron hitting the wall of a plasma. Taking advantage of the large penetration depth at low energies the method factorizes sticking and backscattering probabilities into probabilities for quantum-mechanical transmission and internal backscattering. For the description of the latter we employed an invariant embedding principle. It allows us to extract from the great number of electron trajectories the most important ones which are the trajectories bringing the electron back to the plasma after at least one backscattering but as many forward scattering events as are energetically possible. The approach is applicable to metallic as well as dielectric surfaces. For dielectric surfaces at room temperature, where emission of optical phonons is the dominant scattering process, it is sufficient to include only one backscattering event interlaced in all possible ways between the energetically allowed sequence of forward scattering events.

In this work we focused on SiO_2 and found good agreement with experimental data from electron-beam scattering. Contrary to the perfect absorber assumption, $\bar{S}(E,\xi) \approx 1$, we find energy- and angle-dependent sticking probabilities which can deviate significantly from unity because of internal backscattering due to emission of optical phonons and total reflection due to electron mass mismatch and conservation of total energy and lateral momentum. Angle-averaged sticking probabilities $\langle\bar{S}(E,\xi)\rangle_\xi$ for SiO_2, Al_2O_3, and MgO are also less

than unity. Incorporating the sticking probabilities into orbital-motion limited charging fluxes reduces the grain charge by about 10 percent compared to the perfect absorber value and makes the charge material-dependent.

The method is particularly strong for electron energies below 100 eV. Various scattering mechanism can be included as well as imperfections of the interface. It could thus be used to systematically investigate the interaction of electrons with the walls of low-temperature plasmas. This is indeed required. Electron sticking and backscattering are not universal in the energy range of interest for plasma applications. They have to be studied for each wall material separately.

We acknowledge support by the Deutsche Forschungsgemeinschaft through SFB/TRR 24.

[1] H. M. Mott-Smith and I. Langmuir, Phys. Rev. **28**, 727 (1926).
[2] R. N. Franklin, *Plasma phenomena in gas discharges* (Clarendon Press, Oxford, 1976).
[3] P. Tolias, Plasma Phys. Control. Fusion **56**, 123002 (2014).
[4] M. Bogaczyk, R. Wild, L. Stollenwerk, and H.-E. Wagner, J. Phys. D: Appl. Phys. **45**, 465202 (2012).
[5] R. Tschiersch, M. Bogaczyk, and H.-E. Wagner, J. Phys. D: Appl. Phys. **47**, 365204 (2014).
[6] F. J. J. Peeters and M. C. M. van de Sanden, Plasma Sources Sci. Technol. **24**, 015016 (2015).
[7] I. Richterová, M. Beránek, J. Pavlů, Z. Němeček, and J. Šáfranková, Phys. Rev. B **81**, 075406 (2010).
[8] O. Ishihara, J. Phys. D: Appl. Phys. **40**, R121 (2007).
[9] V. E. Fortov, A. V. Ivlev, S. A. Khrapak, A. G. Khrapak, and G. E. Morfill, Phys. Rep. **421**, 1 (2005).
[10] A. Dunaevsky, Y. Raitses, and N. J. Fisch, Phys. Plasmas **10**, 2574 (2003).
[11] S. Barral, K. Makowski, Z. Peradzyński, N. Gascon, and M. Dudeck, Phys. Plasmas **10**, 4137 (2003).
[12] M. Lapke, T. Mussenbrock, R. P. Brinkmann, C. Scharwitz, M. Boeke, and J. Winter, Appl. Phys. Lett. **90**, 121502 (2007).
[13] J. Cazaux, J. Appl. Phys. **111**, 064903 (2012).
[14] F. Salvat-Pujol and W. S. M. Werner, Surf. Interface Anal. **45**, 873 (2013).
[15] W. S. M. Werner, Surf. Interface Anal. **31**, 141 (2001).
[16] A. Klassen, A. Bauereiss, and C. Koerner, J. Phys. D: Appl. Phys. **47**, 065307 (2014).
[17] L. G. Glazov and S. Tougaard, Phys. Rev. B **68**, 155409 (2003).
[18] E. Schreiber and H.-J. Fitting, J. Electron Spectros. Relat. Phenom. **124**, 25 (2002).
[19] A. Dubus, A. Jablonski, and S. Tougaard, Progr. Surface Science **63**, 135 (2000).
[20] M. Vicanek, Surface Science **440**, 1 (1999).
[21] S. L. Dudarev, P. Rez, and M. J. Whelan, Phys. Rev. B **51**, 3397 (1995).
[22] A. L. Tofterup, Phys. Rev. B **32**, 2808 (1985).
[23] K. Kanaya and S. Okayama, J. Phys. D: Appl. Phys. **5**, 43 (1972).
[24] R. Dashen, Phys. Rev. **134**, A1025 (1964).
[25] M. Shihab, A. T. Elgendy, I. Korolov, A. Derzsi, J. Schulze, D. Eremin, T. Mussenbrock, Z. Donkó, and R. P. Brinkmann, Plasma Sources Sci. Technol. **22**, 055013 (2013).
[26] L. Stollenwerk, S. Amiranashvili, J.-P. Boeuf, and H.-G. Purwins, Eur. Phys. J. D **44**, 133 (2007).
[27] H. Kersten, H. Deutsch, and G. M. W. Kroesen, Int. J. Mass Spectr. **233**, 51 (2004).
[28] R. Brandenburg, V. A. Maiorov, Y. B. Golubovskii, H.-E. Wagner, J. Behnke, and J. F. Behnke, J. Phys. D: Appl. Phys. **38**, 2187 (2005).
[29] D. Uhrlandt, M. Schmidt, J. F. Behnke, and T. Bindemann, J. Phys. D: Appl. Phys. **33**, 2475 (2000).
[30] Y. L. Al'pert, A. V. Gurevich, and L. P. Pitaevskii, *Space physics with artificial satellites* (Consultants Bureau, New York, 1965).
[31] D. A. Mendis, Plasma Sources Sci. Technol. **11**, A219 (2002).
[32] F. X. Bronold and H. Fehske, Phys. Rev. Lett. **115**, 225001 (2015).
[33] T. W. Hickmott, J. Appl. Phys. **36**, 1885 (1965).
[34] L. G. Glazov and I. Pázsit, Nucl. Instr. and Meth. B **256**, 638 (2007).
[35] C. J. Cook and W. J. Fredericks, J. Chem. Phys **36**, 608 (1962).
[36] G. F. Dionne, J. Appl. Phys. **46**, 3347 (1975).
[37] R. L. Heinisch, F. X. Bronold, and H. Fehske, Phys. Rev. B **85**, 075323 (2012).
[38] C. M. Wu and E. S. Yang, Solid-State Electronics **22**, 241 (1979).
[39] T. K. Gaylord and K. F. Brennan, J. Appl. Phys. **65**, 814 (1989).
[40] B. K. Ridley, J. Appl. Phys. **84**, 4020 (1998).
[41] R. Oswald, E. Kasper, and K. H. Gaukler, J. Electron Spectros. Relat. Phenom. **61**, 251 (1993).
[42] V. W. Ballarotto, M. Breban, K. Siegrist, R. J. Phaneuf, and E. D. Williams, J. Vac. Sci. Technol. B **20**, 2514 (2002).
[43] E. Vella, F. Messina, M. Cannas, and R. Boscaino, Phys. Rev. B **83**, 174201 (2011).
[44] D. L. Smith, E. Y. Lee, and V. Narayanamurti, Phys. Rev. Lett. **80**, 2433 (1998).
[45] Y.-S. Kim, S.-H. Yoon, S.-G. Ahn, C.-R. Hong, and H. Yang, Electron. Mater. Lett. **4**, 113 (2008).
[46] A. R. Oganov, M. J. Gillan, and G. D. Price, J. Chem. Phys. **118**, 10174 (2003).
[47] J. Shan, F. Wang, E. Knoesel, M. Bonn, and T. F. Heinz, Phys. Rev. Lett. **90**, 247401 (2003).
[48] E. Bersch, S. Rangan, R. A. Bartynski, E. Garfunkel, and E. Vescovo, Phys. Rev. B **78**, 085114 (2008).
[49] J. E. Allen, Phys. Scripta **45**, 497 (1992).
[50] M. Lampe, R. Goswami, Z. Sternovsky, S. Robertson, V. Gavrishchaka, G. Ganguli, and G. Joyce, Phys. Plasma **10**, 1500 (2003).
[51] S. A. Khrapak, S. V. Ratynskaia, A. V. Zobnin, A. D. Usachev, V. V. Yaroshenko, M. H. Thoma, M. Kretschmer, H. Hoefner, G. E. Morfill, O. F. Petrov, et al., Phys. Rev. E **72**, 016406 (2005).
[52] J. Carstensen, H. Jung, F. Greiner, and A. Piel, Phys. Plasmas **18**, 033701 (2011).